Locomotion Mechanics of Wheeled Rovers on Simulated Lunar Soil

Genya Ishigami, Keiji Nagatani, and Kazuya Yoshida

Department of Aerospace Engineering, Tohoku University

Abstract : In this paper, locomotion mechanics for a lunar exploration rover are addressed. The authors have developed mathematical models to evaluate the longitudinal and lateral traction forces of a wheel for various slip conditions, and the model has been quantitatively verified using a single wheel test bed. The wheel model for locomotion mechanics has been incorporated into an articulated multibody model of the entire rover in order to describe the motion dynamics of the rover. The experiments using a four-wheel rover for horizontal steering and slope traversing have been carried out. The proposed model for an analysis of locomotion mechanics of the rover is verified through comparison between the experimental result and simulation result using the proposed model.

車輪型ローバーの模擬月面土壌における走行特性の研究

石上 玄也 永谷 圭司 吉田 和哉

東北大学大学院 工学研究科 航空宇宙工学専攻

概要：筆者らの研究グループでは，模擬月面土壌（レゴリスシミュラント）を用いて，車輪型ローバーの走行特性の研究をおこなっている．様々なスリップ状態における車輪の縦方向および横方向の駆動力を評価するモデルを構築し，車輪走行試験装置を用いて車輪モデルの定量的評価をおこなってきた．また，４車輪ローバーモデルを開発し，ローバーのステアリング特性や斜面横断時の走行特性を明らかにするとともに，数値シミュレーションモデルとの比較をおこなってきた．本稿では，これまでの研究成果の概要を報告する．

1. Introduction

The surface terrain of the Moon is largely covered with a fine-grained loose soil called *regolith*. On such loose soil, the wheels of a lunar exploration rover easily slip and lose traction. Therefore, investigations on the contact and traction mechanics between wheels and soil are necessary in order to better understand the motion behavior of a rover on loose soil.

Wheel-soil interaction mechanics have been well studied in the field of *terramechanics*. In this field, the principle of the wheel-soil interaction mechanics and the empirical models of the stress distributions beneath the wheels have been previously investigated [1]-[3]. Recently, these terramechanics-based models have been successfully applied to the motion analysis of planetary rovers [4]. We have developed a terramechanics-based dynamics model for exploration rovers by considering the slip and traction forces of a rigid wheel on loose soil [5][6]. Further, the authors have also elaborated upon a wheel-and-vehicle model to address the motion dynamics of the rover [7][8].

In this paper, locomotion mechanics of lunar exploration rovers are addressed for numerical analyses of motion behaviors of the rover. This research studies two models to deal with the motion behaviors. First, a wheel-soil contact model is developed to deal with the wheel slip/skid behaviors, and subsequently, the motion dynamics of the rover are numerically obtained by using a wheel-and-vehicle model.

The wheel-soil contact model enables calculation of 3-axis wheel forces, namely drawbar pull, side force, and vertical force. Then, the relationships among the slip ratio (a measure of the longitudinal slip), slip angle (a measure of the lateral slip), drawbar pull, and side force are derived. The validity of the wheel-soil contact model and the theoretical relationships is confirmed through experiments using a single-wheel test bed. In these experiments, *lunar regolith simulant* is utilized, which simulates the soil on the lunar surface.

The motion behavior of the entire rover is numerically evaluated by using a wheel-and-vehicle model in which the wheel-soil model is incorporated into an articulated multibody model for describing the motion dynamics of the vehicle's body and chassis. The simulation results obtained with the wheel-and-vehicle model are compared with the results of experiments conducted using a four-wheeled rover test bed on the lunar regolith simulant. The experiments on horizontal steering and slope traversing are carried out.

This paper is organized as follows: the following section, Section 2, describes the models for the wheel-soil contact mechanics. The single wheel experiments and numerical simulations are described in Section 3 along with a discussion on the validity of the wheel-soil models. In Section 4, the model for the wheel-and-vehicle dynamics is introduced. The experiments using a rover test bed are addressed in Section 5, and the validity of the proposed model is then discussed.

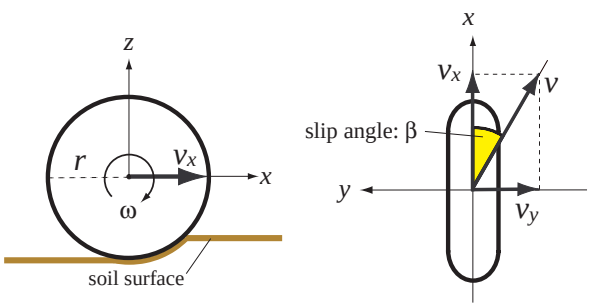

Fig. 1: Wheel coordinate system

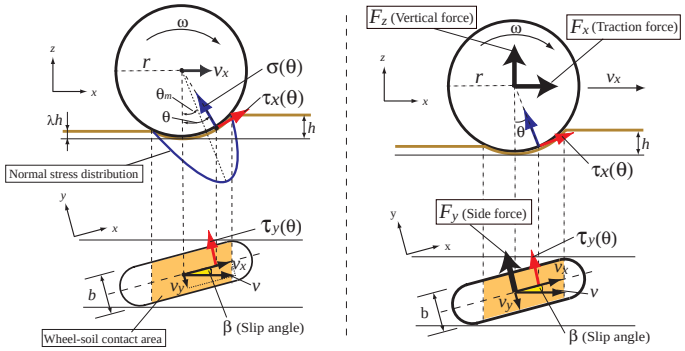

(a) : Stress model (b) : Force model

Fig. 2: Wheel-soil contact model

2. Wheel-Soil Contact Model

The following analysis concerns a rigid wheel rotating on loose soil. A wheel coordinate system is defined using a right-hand frame, as shown in Fig. 1; in this system, the longitudinal direction is denoted by x, the lateral direction by y, and the vertical direction by z. The coordinate frame rotates according to the steering action of the wheel (the yaw rotation around the z axis) but does not rotate with the driving motion of the wheel (the pitch rotation around the y axis).

2.1 Slip ratio and slip angle

Slips are generally observed when a rover travels on loose soil. In addition, during steering or slope-traversing maneuvers, slips in the lateral direction are also observed. The slip in the longitudinal direction is expressed by the slip ratio s, which is defined as a function of the longitudinal traveling velocity of the wheel v_x and the circumference velocity of the wheel $r\omega$ (r is the wheel radius and ω represents the angular velocity of the wheel)

$$s = \begin{cases} (r\omega - v_x)/r\omega & (\text{if } |r\omega| > |v_x| : \text{driving}) \\ (r\omega - v_x)/v_x & (\text{if } |r\omega| < |v_x| : \text{braking}). \end{cases} \quad (1)$$

The slip ratio assumes a value in the range from -1 to 1.

On the other hand, the slip in the lateral direction is expressed by the slip angle β, which is defined by using v_x and the lateral traveling velocity v_y as follows:

$$\beta = \tan^{-1}(v_y/v_x). \quad (2)$$

2.2 Wheel stress distribution

When a wheel rotates on loose soil, normal and shear stresses are generated under the wheel. These stresses are quite necessary to calculate wheel forces. Based on terramechanics models, the stresses under a rotating wheel can be modeled as shown in Fig. 2-(a).

The normal stress $\sigma(\theta)$ is determined by the following equation [5]:

$$\sigma(\theta) = \begin{cases} r^n \left(\frac{k_c}{b} + k_\phi\right) [\cos\theta - \cos\theta_f]^n & (\theta_m \le \theta < \theta_f) \\ r^n \left(\frac{k_c}{b} + k_\phi\right) \left[\cos\{\theta_f - \frac{\theta - \theta_r}{\theta_m - \theta_r} \right. \\ \qquad \left. (\theta_f - \theta_m)\} - \cos\theta_f\right]^n & (\theta_r < \theta \le \theta_m), \end{cases} \quad (3)$$

where, θ_f and θ_r are the entry and exit angles, respectively. The wheel contact patch on loose soil is defined by the region between the entry and exit angles. k_c, k_ϕ, and n are the soil-specific parameters. b is the width of wheel. Further, θ_m is the specific wheel angle at which the normal stress is maximized:

$$\theta_m = (a_0 + a_1 s)\theta_f, \quad (4)$$

where a_0 and a_1 are parameters that depend on the wheel-soil interaction. Their values are generally assumed as $a_0 \approx 0.4$ and $0 \le a_1 \le 0.3$ [9].

The shear stresses $\tau_x(\theta)$ and $\tau_y(\theta)$ are expressed using identical expressions [10]:

$$\tau_x(\theta) = (c + \sigma(\theta)\tan\phi)[1 - e^{-j_x(\theta)/k_x}], \quad (5)$$
$$\tau_y(\theta) = (c + \sigma(\theta)\tan\phi)[1 - e^{-j_y(\theta)/k_y}]. \quad (6)$$

In these equations, c represents the cohesion stress of the soil; ϕ, the internal friction angle of the soil; and k_x and k_y, the shear deformation modules.

Further, j_x and j_y, which are the soil deformations, can be formulated as functions of the wheel angle θ [6][9]:

$$j_x(\theta) = r[\theta_f - \theta - (1-s)(\sin\theta_f - \sin\theta)], \quad (7)$$
$$j_y(\theta) = r(1-s)(\theta_f - \theta)\cdot\tan\beta. \quad (8)$$

2.3 Drawbar pull : F_x

A general force model for a rigid wheel on loose soil is presented in Fig. 2-(b). Using the normal stress $\sigma(\theta)$ and the shear stress in the x direction $\tau_x(\theta)$, the drawbars pull F_x, which acts in the direction from the soil toward the wheel, is calculated by integrating from the entry angle θ_f to the exit angle θ_r [9]:

$$F_x = rb\int_{\theta_r}^{\theta_f} \{\tau_x(\theta)\cos\theta - \sigma(\theta)\sin\theta\} d\theta. \quad (9)$$

2.4 Side force : F_y

The side force F_y acts along the lateral direction of a wheel when the vehicle makes a steering maneuver. We model the side force as follows [6]:

$$F_y = \int_{\theta_r}^{\theta_f} \{rb\cdot\tau_y(\theta) + R_b\cdot(r - h(\theta)\cos\theta)\} d\theta. \quad (10)$$

R_b is the reaction resistance generated by the bulldozing phenomenon on the side face of the wheel. R_b is given as a function of a wheel sinkage h. Detailed formulation of the side force can be seen in [8].

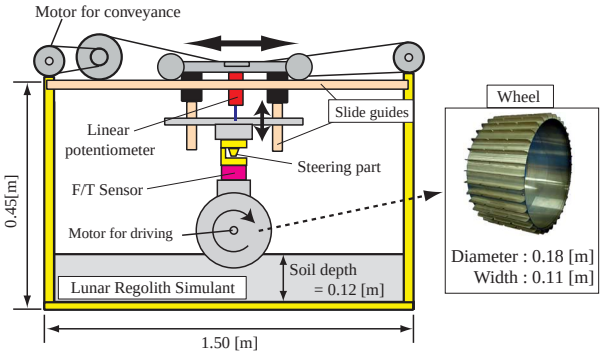

Fig. 3: Schematic view of the single wheel test bed

2.5 Vertical force : F_z

The vertical force should be equal to the normal load of the wheel. The vertical force F_z is obtained by the same method as described in equation (9) [9]:

$$F_z = rb \int_{\theta_r}^{\theta_f} \{\tau_x(\theta) \sin\theta + \sigma(\theta) \cos\theta\} d\theta. \qquad (11)$$

3. Single Wheel Experiment and Simulation

Single wheel experiments are carried out to validate the wheel-soil contact model. The experimental results are compared to numerical simulation results obtained from the wheel-soil contact model. In particular, the characteristics of both the drawbar pull and the side force were confirmed.

3.1 Single wheel test bed

Fig. 3 shows the schematic view of the single wheel test bed. The test bed comprises both a conveyance unit and a wheel-driving unit. The steering angle (which is equivalent to the slip angle in this test bed) is set between the conveyance unit and the wheel. The translational velocity and angular velocity of the wheel are calculated based on the data obtained by the encoders that are mounted on the conveyance motor and wheel-driving motor, respectively. The forces and torques generated by the wheel locomotion are measured using a six-axis force/torque sensor located between the steering part and the wheel. The wheel sinkage is also measured by using a linear potentiometer. A wheel with a diameter of 0.18 [m] and a width of 0.11 [m] is covered with paddles having heights of 0.01 [m]. The load of the wheel is approximately 6.6 [kg].

The vessel of the single-wheel test bed is filled with 12 [cm] (depth) of loose soil, *lunar regolith simulant* which is equivalent to *FJS-1* [11]. The simulated lunar soil consists of material components and mechanical characteristics similar to those of the real lunar soil.

In the following experiments, the wheel is made to rotate with a controlled constant velocity (0.030 [m/s]) by the driving motor, which is mounted inside the wheel. The translational velocity of the wheel is also controlled such that the slip ratio of the wheel is set from 0.0 to 0.8 in steps of 0.1. The slip ratio is constant during each run. Further, the value of the slip angle of the wheel is varied from 5° to 30°. Multiple test runs were conducted for a single set of the above-mentioned conditions; the total number of runs was more than 100. In addition, during each run, more than 100 data points were extracted for the analysis.

Table 1: Simulation parameters and values

parameter	value	unit
c	0.80	[kPa]
ϕ	37.2	[deg]
k_c	1.37×10^3	[N/m^{n+1}]
k_ϕ	8.14×10^5	[N/m^{n+2}]
n	1.00	
k_x	$0.043 \times \beta + 0.036$	[m]
k_y	$0.020 \times \beta + 0.013$	[m]

3.2 Numerical simulation procedure

The simulations using the wheel-soil contact model were performed under the same conditions as those of the single-wheel experiments. The parameters used in the simulations are listed in Table 1. Each parameter is experimentally determined. The drawbar pull and side force are calculated by equations (9) and (10), respectively.

3.3 Results and discussion

Experimental measurements of the drawbar pull and side force are plotted in Fig. 4-(a) and Fig. 4-(b), respectively, for each slip angle from 5° to 30°. As mentioned above, hundreds of data points were obtained from a single test run. Each plot corresponds to the average value of these data points. The theoretical curves calculated by the wheel-soil contact model are also plotted in these figures.

From Fig. 4-(a), it is seen that the drawbar pull increases with the slip ratio. The reason for this behavior is that the soil deformation (shear stress) in the longitudinal direction of the wheel increases with the slip ratio. This results in a large soil deformation which, in turn, generates a large drawbar pull. In the range of slip ratios from 0 to 0.3, the drawbar pull becomes smaller with increasing slip angles. This is because the shearing motion in the longitudinal direction decreases as the lateral slip (slip angle) increases.

The differences between the experimental and theoretical values are relatively small in the range of slip angles from 5°-20°; however, relatively larger differences are observed for larger slip angles ($\geq 25°$). The reason for this is considered that the soil beneath the wheel becomes fluidized and different mechanics may dominate the phenomena in high slip ratio and high slip angle conditions. In practice, however, such large slip angles are rarely experienced under normal steering maneuvers.

Fig. 4-(b) shows that the side force decreases along with the slip ratio and increases according to the slip angle. The larger the slip angle, the larger the lateral velocity on the wheel, which leads to a larger side force. In addition, it is observed that the side force has its maximum value at $s = 0.0$ because the lateral

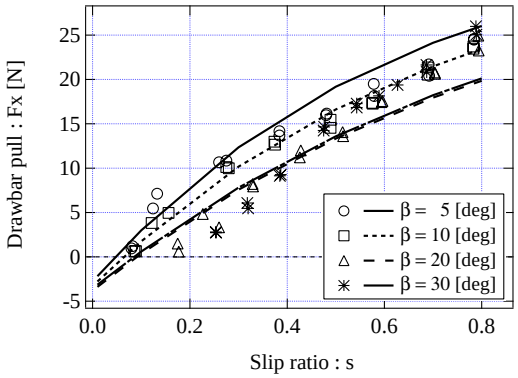

(a) : Slip ratio - Drawbar pull

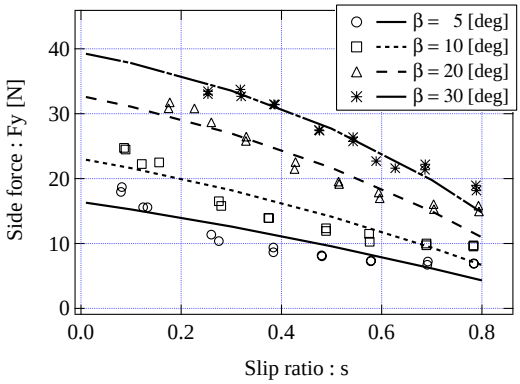

(b) : Slip ratio - Side force

Fig. 4: Experimental and simulation results

velocity, in proportion to the longitudinal velocity, is maximized at $s = 0.0$ for each slip angle. The theoretical curves agree well with the plotted experimental results.

These results confirm that the wheel-soil contact model proposed in this paper is able to represent the motion behavior of the wheel and the contact/traction forces with appropriate accuracy.

4. Wheel-and-Vehicle Model

To describe the motion dynamics of the rover, a wheel-and-vehicle model is developed. In this model, the rover is modeled as an articulated body system to calculate the motion dynamics of its body and chassis. Furthermore, the contact forces on each wheel of the rover can be obtained by using the wheel-soil contact model.

4.1 Rover test bed

The vehicle in the simulation was tested in our rover test bed, as shown in Fig. 5. The rover test bed has the dimensions 0.68 [m] (length) × 0.44 [m] (width) × 0.32 [m] (height) and weighs approximately 35 [kg] in total. Each wheel has the same configuration as that in the single-wheel experiments.

4.2 Definition of wheel-and-vehicle model

The dynamics model of the rover shown in Fig. 5 is completely equivalent to the rover test bed.

The dynamic motion of the rover for given traveling

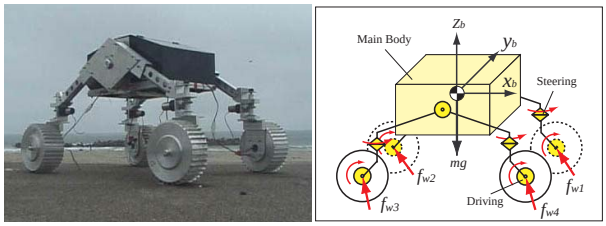

(Rover test bed) (Vehicle dynamics model)

Fig. 5: Rover test bed and vehicle dynamics model

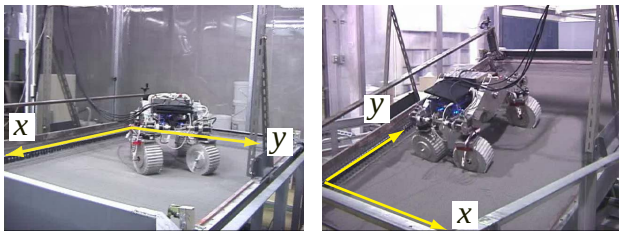

(a) : Steering experiment (b) : Slope traversing experiment

Fig. 6: Experimental overviews

and steering conditions are numerically obtained by successively solving the following motion equation:

$$\boldsymbol{H}\begin{bmatrix}\dot{\boldsymbol{v}}_0\\ \dot{\boldsymbol{\omega}}_0\\ \ddot{\boldsymbol{q}}\end{bmatrix} + \boldsymbol{C} + \boldsymbol{G} = \begin{bmatrix}\boldsymbol{F}_0\\ \boldsymbol{N}_0\\ \boldsymbol{\tau}\end{bmatrix} + \boldsymbol{J}^T\begin{bmatrix}\boldsymbol{F}_e\\ \boldsymbol{N}_e\end{bmatrix}, \quad (12)$$

where $\boldsymbol{H}$ represents the inertia matrix of the rover; $\boldsymbol{C}$, the velocity depending term; $\boldsymbol{G}$, the gravity term; $\boldsymbol{v}_0$, the translational velocity of the main body; $\boldsymbol{\omega}_0$, the angular velocity of the main body; $\boldsymbol{q}$, the angle of each joint of the rover; $\boldsymbol{F}_0$ and $\boldsymbol{N}_0$, the external forces and moments acting at the centroid of the main body; $\boldsymbol{\tau}$, the torques acting at each joint of the rover; $\boldsymbol{J}$, the Jacobian matrix; $\boldsymbol{F}_e = [f_{w1}, \ldots, f_{wm}]$, the external forces acting at the centroid of each wheel; $\boldsymbol{N}_e$, the external moments acting at the centroid of each wheel.

Note that each external force $\boldsymbol{f}_{wi}$ is calculated by the wheel-soil contact model, as mentioned in Section 2. The subscript i denotes the number of wheels (in this case, i=1, ..., 4).

5. Experiment using Rover Test Bed

The experiments on horizontal steering and slope traversing were conducted in order to validate the wheel-and-vehicle model. The dynamics simulations using the proposed model were also carried out and the simulation results were compared to the corresponding experiments.

5.1 Experimental setup

Fig. 6 shows overviews of the experimental setup with our rover test bed. The test field, located at Japan Aerospace Exploration Agency (JAXA), consists of a flat rectangular vessel measuring 1.5 × 2.0 [m], evenly filled with 10 [cm] (depth) of the lunar regolith simulant. The vessel can be inclined up to 30 [deg].

The rover test bed travels with a given angular ve-

Table 2: Experimental conditions

(a) Steering experiment

Case	[deg]	
	Front	Rear
a	15	0
b	30	0

(b) Slope traversing Experiment

Case	[deg]	
	Front	Rear
A	0	0
B	15	0
C	15	15

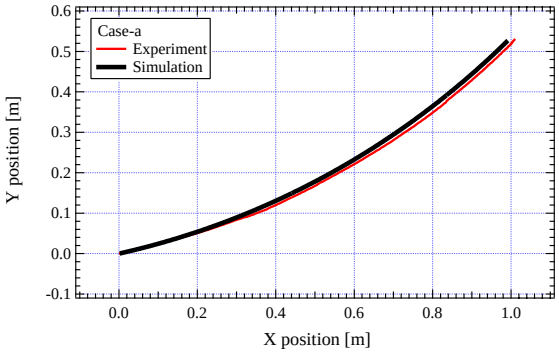

(a) case-a

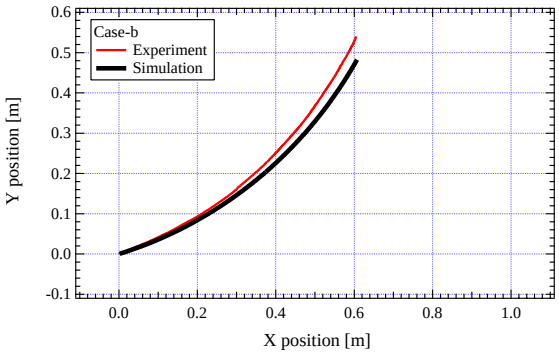

(b) case-b

Fig. 7 : Comparison of the simulated and experimental steering trajectories

locity and steering angle. Each wheel is controlled to travel with a constant wheel angular velocity and steering angle by an on-board computer. In every experiment, the given angular velocity of each wheel was maintained at 0.3 [rad/s] (2.86 [rpm]). The average traveling velocity of the rover was around 0.03 [m/s]. The steering trajectories of the rover are measured using a 3D optical sensor system fixed on the ceiling.

5.2 Steering experiment and discussion

The conditions for two typical cases in the steering experiments are listed in Table 2-(a): in case-a, the steering angles of the left and right front wheels were fixed at 15°, whereas, in case-b, they were fixed at 30°. The steering angles of the left and right rear wheels were 0° in both cases.

The experimental results regarding the steering trajectories of the rover are shown in Fig. 7-(a) and Fig. 7-(b). The steering trajectories obtained from the wheel-and-vehicle model are also plotted in the same figures.

From Fig. 7, it can be observed that the wheel-and-vehicle model well simulates the experimental results. Taking into account wheel slippage, the proposed model calculates better steering trajectories, which almost agree with the experimental results. The root mean square (RMS) error of the proposed model is negligible (less than 0.04 [m]). The accuracy of the proposed model is better than 0.06 [m] (less than the wheel width) even in the final state. The proposed model simulates the experimental steering trajectories with relatively better accuracy from the viewpoint of the error percentages.

Throughout the experiments, it was observed that the slip ratios were in the range from 0.1 to 0.3 and the slip angles were in the range from $-7°$ to $15°$. Despite such dynamic wheel behavior, our model is able to calculate the wheel slippage and the steering motion of the rover with a remarkably good accuracy.

5.3 Slope traversing experiment xand discussion

In the experiment, the rover is given three different steering configurations as listed in Table 2-(b): in case-A, no steering anlges were given to any wheels, in case-B, the steering angles of the front wheels were fixed at 15°, whereas the rear wheels were 0°, and in case-C, every steering angle was fixed at 15°. Further, the slope angle was given from 5° to 15° in steps of 5°.

The experimental results regarding the slope traversing trajectories of the rover are shown in Fig. 8 with different slope anlges. The trajectories obtained from the wheel-and-vehicle model are also plotted in the same figures.

From Fig. 8, in both case-A and case-C, it can be seen that the trajectories calculated by the wheel-and-vehicle model agree well with the corresponding experimental results. The errors between the experiment and simulation are less than a few percents in regard to the total travel distance of the rover. The proposed model can simulate such dynamic behavior on slopes of loose soil.

It is found that there is relatively large error in case-B when the rover traversed on slopes of 10 [deg] and 15 [deg]. This error is considered to be due to the modeling error of the vehicle dynamics model. In the simulation, the rover is modeled as an articulated body system, and then, each part of the rover is assumed to have completely rigid connections with adjacent parts. The rover test bed has a flexible suspension mechanism and this mechanism is also modeled as a spring-damper model. However, the deformation of this suspension became much larger than the model expects since the cornering force of the rover in case-B was larger than that in the other cases. Then, it is deduced that dynamics parameters for the suspension was not appropriate so that the large error of the trajectory must be generated. Note that this issue can be improved once the suspension mechanism in the vehicle dynamics model is refined so as to correspond with the suspension of the rover.

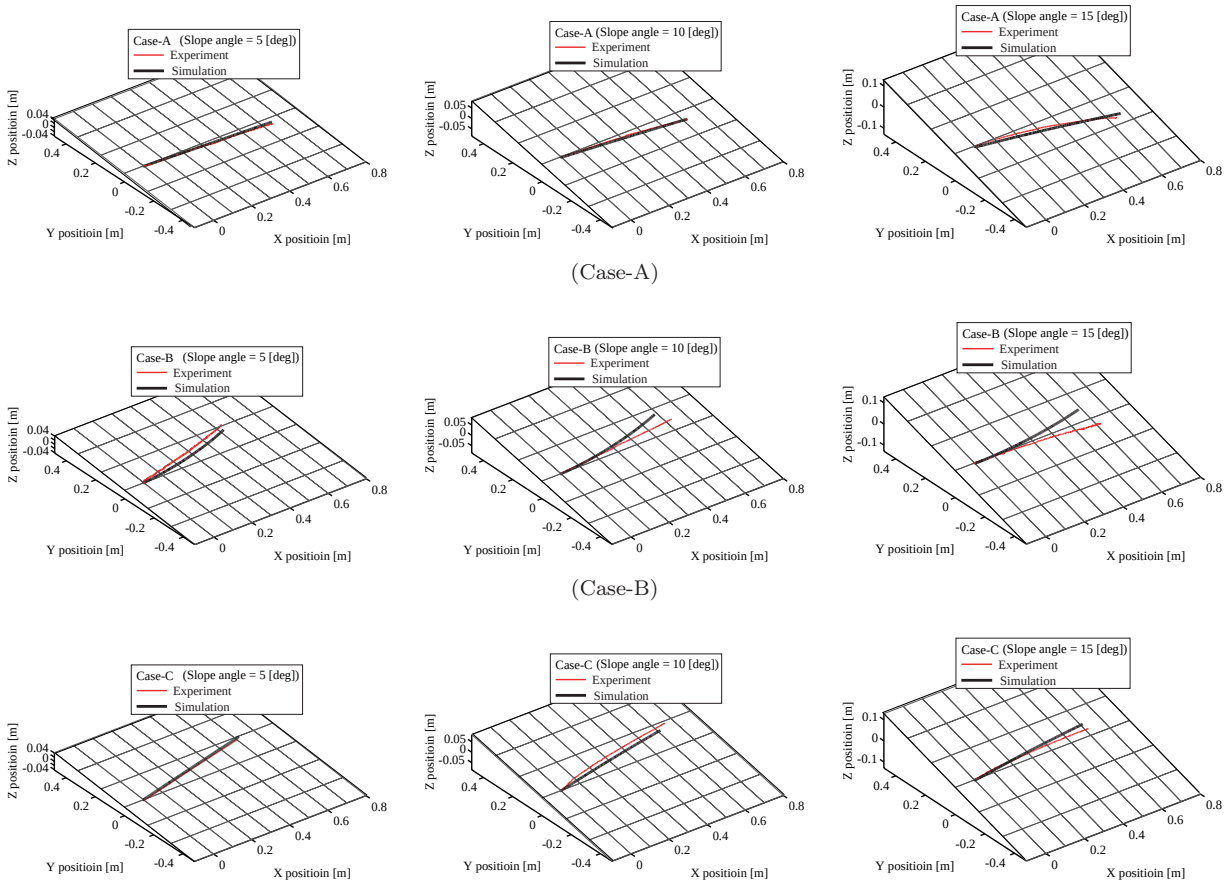

(Case-A)

(Case-B)

(Case-C)

Fig. 8: Comparison of the simulated and experimental trajectories on slope traversing

6. Conclusion

In this paper, locomotion mechanics of lunar exploration rovers has been addressed for numerical analyses of motion behaviors of the rover. To deal with dynamic motion behavior of the rover, the wheel-and-dynamics model has been developed. The proposed model consists of two models. The wheel-soil contact model has been developed to calculate the slip/skid of wheels rotating on loose soil, and subsequently, the motion dynamics of the rover have been numerically obtained by incorporating the wheel-soil contact model into the vehicle dynamics model.

The wheel-soil contact model has been developed based on terramechanics and then quantitatively verified using a single wheel test bed. In addition, through the comparison between experiment and simulation, it has been confirmed that the wheel-and-vehicle model demonstrates good accuracy in predicting motion behaviors.

The models developed in this paper are useful in performing off-line computation of the vehicle motion trajectories under slipping/skidding conditions. Further, the model can also be applied to evaluate the performance of the vehicle's climbing/traversing capabilities.

Acknowledgment

The authors would like to express their best thanks to Dr. K. Matsumoto and Dr. S. Wakabayashi at Japan Aerospace Exploration Agency (JAXA), for providing opportunities of the steering experiments using their facility.

References

[1] M. G. Bekker; *Off-The-Road Locomotion*, The University of Michigan Press, 1960.

[2] M. G. Bekker; *Introduction to Terrain-Vehicle Systems*, The University of Michigan Press, 1969.

[3] J. Y. Wong; *Theory of Ground Vehicles*, John Wiley & Sons, 1978.

[4] K. Iagnemma and S. Dubowsky; *Mobile Robot in Rough Terrain*, Springer Tracts in Advanced Robotics, vol.12, 2004.

[5] K. Yoshida, T. Watanabe, N. Mizuno, and G. Ishigami; "Terramechanics-Based Analysis and Traction Control of a Lunar/Planetary Rover," *4th Int. Conf. on Field and Service Robotics,* July 2003.

[6] K. Yoshida and G. Ishigami; "Steering Characteristics of a Rigid wheel for Explaration on Loose Soil," *Proc. of the 2004 IEEE Int. Conf. on Intelligent Robots and Systems,* pp. 3995–4000, 2004.

[7] G. Ishigami and K. Yoshida; "Steering Characteristics of an Exploration Rover on Loose Soil Based on All-Wheel Dynamics Model," *Proc. of the 2005 IEEE Int. Conf. on Intelligent Robots and Systems,* pp. 2041-2046, 2005.

[8] G. Ishigami, A. Miwa, K. Nagatani, and K. Yoshida; "Terramechanics-Based Model for Steering Maneuver of Planetary Exploration Rovers on Loose Soil," *The Journal of Field Robotics,*, Vol. 24, No. 3, 2007, pp. 233-250.

[9] J. Y. Wong and A. Reece; "Prediction of rigid wheel prefoemance based on the analysis of soil-wheel stresses (part I preformance of driven rigid wheels)," *Journal of Terramechanics*, Vol. 4, 1967pp. 81-98.

[10] Z. Janosi and B. Hanamoto; "The analytical determination of drawbar pull as a funcition of slip for tracked vehicle in deformable soils," *Proc. of the 1st Int. Conf. on Terrain-Vehicle Systems*, 1961.

[11] H. Kanamori, S. Udagawa, T. Yoshida, S. Matsumoto, and K. Takagi; "Properties of lunar soil simulant manufactured in Japan," *Proc. of the 6th Int. Conf. and Exposition on Engineering, Construction, and Operations in Space*, 1998.